Pergamon

Geochimica et Cosmochimica Acta, Vol. 62, No. 18, pp. 3131–3139, 1998

0016-7037/98 $19.00 + .00

PII S0016-7037(98)00212-9

Measurement of oxygen fugacities under reducing conditions: Non-Nernstian behavior of Y_2O_3-doped zirconia oxygen sensors

R. A. MENDYBAEV,[1] J. R. BECKETT,[2,*] E. STOLPER,[2] and L. GROSSMAN[1]

[1]Department of Geophysical Sciences, University of Chicago, Chicago, Illinois 60637, USA
[2]Division of Geological and Planetary Sciences, California Institute of Technology, Pasadena, California 91125, USA

(*Received June* 9, 1997; *accepted in revised form June* 8, 1998)

Abstract—A calibration procedure is presented for the use of a Y_2O_3-stabilized zirconia (YSZ) oxygen sensor in 1 atm gas-mixing furnaces in the temperature range 1200–1500°C and 0–8 orders of magnitude below the iron-wüstite (IW) buffer. Corrections to the Nernst equation were obtained by measuring apparent oxygen fugacities of gases in equilibrium with graphite (equilibrated with pure CO vapor), Cr + Cr_2O_3, and Ta + Ta_2O_5. Under reducing conditions, f_{O_2}s calculated using the ideal form of the Nernst equation are erroneously high, by <0.1 log units at IW but by nearly three log units for Ta-Ta_2O_5 at 1000°C.

The deviations between measured emfs and those calculated assuming Nernstian behavior of the electrolyte in the oxygen sensor reflect mixed ionic-electronic conduction. Measured emfs under reducing conditions are readily corrected for this effect via experimentally determined values of P_θ, the oxygen fugacity at which electronic conduction constitutes half of the total conductivity. For the oxygen sensors used in this study,

$$\log P_\theta(\pm 0.20,1\sigma) = 3.70(\pm 0.72) - \frac{(32.95 \pm 1.15)\times 10^3}{T(K)}.$$

Even under conditions more reducing than a gas of solar composition ($f_{O_2} = 10^{-18}$ at 1200°C), YSZ oxygen sensors can be used to determine absolute values of the oxygen fugacity to within ±0.2 log units.

1. INTRODUCTION

Redox conditions play an important role in the evolution of igneous systems, influencing the compositions of individual phases, the speciation within them, and even whether or not a specific phase will be stable. Given observed compositions of minerals, it is often possible to constrain the oxygen fugacity (f_{O_2}) at which they were established, but only if the thermodynamic properties of the phases involved are adequately characterized. Yttrium oxide- (YSZ) and calcium oxide-doped (CSZ) zirconia oxygen sensors are an integral part of the required experimental measurements. They are used (1) to determine directly the free energy of oxidation reactions (Kiukkola and Wagner, 1957; O'Neill et al., 1989; Pratt, 1990), (2) as oxygen sensors (Weissbart and Ruka, 1961; Sato, 1971) to determine the oxygen fugacity of a gas to which a sample is exposed (Huebner, 1987), and (3) for intrinsic oxygen fugacity measurements on mineral grains from natural assemblages (Sato, 1972; Arculus and Delano, 1981; Brett and Sato, 1984; Kozul et al., 1988). In addition, although typically used at a total pressure of 1 atm, it is also possible to use solid oxide electrolytes at elevated pressures (Woermann et al., 1982; Jacob and Iwase, 1983; Yasuda and Fujii, 1993).

Usually underlying each of the above applications are two key assumptions: (1) conduction within the electrolyte is purely ionic and, therefore, (2) the Nernst equation holds in its ideal (i.e., purely ionic) form. Under very oxidizing (oxygen partial pressures exceeding 100 atm for YSZ, Park and Blumenthal, 1989) and reducing (below the IW buffer for YSZ, Etsell and Flengas, 1970) conditions, however, electronic conduction becomes important, and both assumptions become invalid. In this study, we present a simple procedure for correcting measurements using Y_2O_3-stabilized zirconia oxygen sensors so that oxygen fugacities can be determined accurately (±0.2 log units) even under extremely reducing conditions (i.e., f_{O_2}s several orders of magnitude below the IW buffer). We determined the corrections necessary for an SIRO$_2$© oxygen sensor, which is constructed from an alumina (50 wt%) plus YSZ electrolyte plug inserted into an alumina tube and welded to form a gas tight seal. This design contrasts with the more common slip cast electrolyte tubes composed entirely of electrolyte, and, therefore, although our procedures can be used for other types of oxygen sensors, our experimental results should not be applied to them. We also note that our procedures are designed for experiments conducted at elevated temperatures (above ~1200°C), but, given evidence of the systematic behavior of oxygen sensors to lower temperatures (see Ulmer, 1984; Burkhard and Ulmer, 1995; Beckett and Mendybaev, 1997), it should be possible to extrapolate our results to lower temperatures. We note that there are numerous studies using a variety of techniques in the literature concerning the conductivity of solid oxide electrolytes (e.g., Etsell and Flengas, 1970; Worrell, 1977; Iwase et al., 1984a, 1984b; van Wijngaarden et al., 1988; Pratt, 1990; Ramanarayanan et al., 1991; Swider et al., 1991; Naito and Arashi, 1992; Wu et al., 1992; Pandit et al., 1994; Rommerskirchen et al., 1994; Sutija et al., 1995), and we use the same formalism (Schmalzried, 1962, 1963) to describe our results. Our measurements are, however, obtained from an in-use oxygen sensor. They are only indirect indicators of electronic conductivity in the electrolyte but give directly the

*Author to whom correspondence should be addressed (john@expet.gps.caltech.edu).

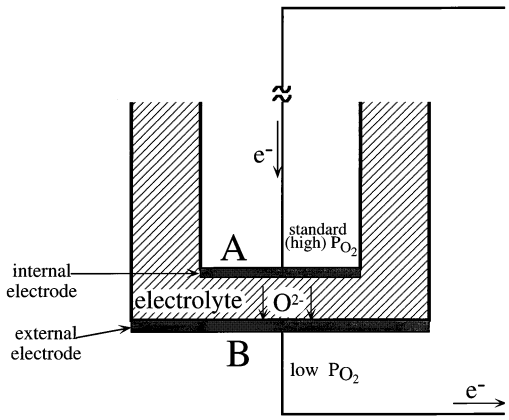

Fig. 1. Schematic of oxygen sensor. Modified after Sato (1971). Labelling of the direction of electron (e^-) and O^{2-} flow follows from assuming that the vapor in contact with interface A has the higher oxygen potential.

necessary corrections for obtaining oxygen fugacities from measured emfs.

1.1. Oxygen Sensors Operating in the Nernstian Regime

In a perfect crystalline oxide (i.e., with no defects), the ions would be restricted to specific lattice sites with only extremely rare jumps between adjacent sites. There are, however, some solids characterized by high concentrations of highly mobile ionic defects that move from one lattice site to another or between lattice sites and interstitial positions with relative ease. When such materials are exposed to an electric field, the mobile defects (anions or cations) migrate in the direction of the applied field while maintaining local electrical neutrality within the solid via charge compensating holes and electrons. This phenomenon is referred to as ionic conduction, and the material within which this occurs is called a solid electrolyte. As a practical working definition (e.g., Alcock, 1993), solid electrolytes are generally restricted to materials for which >99% of the total conductivity is due to ionic conduction. There are many types of solid electrolytes, with mobile ions including F^-, Ca^{2+}, Na^+, H^+, and O^{2-} (Etsell and Flengas, 1970; Pratt, 1990; Iwahara and Hibino, 1993). If the applied field is fixed, the mobile ions can be selectively "pumped" through the solid electrolyte. If the chemical potential of the mobile species is fixed but different on both sides of the solid electrolyte, an electric field is produced within the electrolyte, the magnitude of which is related to the difference in chemical potentials. Thus, for example, when the transport is dominated by oxygen ions, the relationship between an observed emf across the solid electrolyte and the difference in the chemical potential (or, equivalently, the oxygen fugacity) across the electrolyte can become very simple and can be used to measure accurately the difference in f_{O_2} between the two sides of the electrolyte.

Figure 1 is a schematic representation of an oxygen sensor (e.g., with an electrolyte made of YSZ). Two gases, each at equilibrium (i.e., with a well defined partial pressure of oxygen), are separated by the solid electrolyte, with electrodes attached to both surfaces of the electrolyte. Generally, this requires an effectively infinite reservoir for each gas, which is generated by constantly flowing vapor. Provided that (1) charge transfer across the electrolyte occurs strictly by the flow of oxygen anion defects (O^{2-}; i.e., the dominant defects are doubly ionized oxygen vacancies), (2) the meter in the electrical circuit connecting the two electrodes used to measure the voltage has a very large resistance, and (3) there are no chemical reactions or diffusive fluxes causing a significant change in the compositions of the gases, the electrolyte, or the electrodes, then there will be no net flow of current or mass across either electrode/electrolyte interface. Under these conditions, the cell shown in Fig. 1 is reversible and, if the f_{O_2} at interface A is different from that at B, the chemical potential difference will cause a corresponding but opposite electrical potential difference in the electrons at the two electrodes. Provided that the electrodes and electrical leads are of the same material (e.g., W, Pt), there will be no thermal emf caused by differing resistivities, and the potential difference between the two electrodes can be described by (e.g., Kingery et al., 1976)

$$E_{cell} = \frac{-RT}{4F} \ln\left(\frac{f_{O_2@B}}{f_{O_2@A}}\right), \quad (1)$$

where F is the Faraday constant (96484 J/V), R the gas constant, T the absolute temperature, and f_{O_2}@i the oxygen fugacity at interface *i*. Equation 1 is known as the Nernst equation. By introducing a gas of known oxygen fugacity at A and measuring the cell emf, it is possible through Eqn. 1 to determine the oxygen fugacity of a gas of unknown composition at B. In 1 atm gas-mixing experiments, the standard f_{O_2} is generally fixed by air or pure oxygen, although it is also possible to use solid buffer assemblages (e.g., Cu + Cu_2O or Fe + $Fe_{1-x}O$) to fix the standard f_{O_2}.

1.2. Oxygen Sensors Operating under Non-Nernstian Conditions

The total conductivity of stabilized zirconia incorporates contributions from oxygen vacancies, electrons, and holes. The conductivity, σ_i, due to oxygen vacancies is independent of oxygen fugacity, being dictated primarily by dopant concentrations, but those of electrons ($\sigma_{e^-} \propto f_{O_2}^{-1/4}$) and holes ($\sigma_h \cdot \propto f_{O_2}^{+1/4}$) (see e.g., Patterson, 1971; Worrell, 1977) are not. Under sufficiently reducing conditions, transport of free electrons (n-type conduction) becomes important and, at high f_{O_2}s, electron holes (p-type conduction) dominate the total conductivity (under even more extreme conditions, other dependencies on the total conductivity may be expected, e.g., Smyth, 1976, 1977; Kofstad, 1983; Subbarao and Maiti, 1984). Thus, in either regime, an assumption implicit in the derivation of the ideal form of the Nernst equation given by Eqn. 1, that ionic conduction is the dominant mode of charge transfer across the electrolyte, begins to break down. This electronic conduction partially short circuits the cell shown in Fig. 1 so that E_{cell} will be lower than expected on the basis of Eqn. 1. If the Nernst equation is used in its standard form under these conditions, the predicted difference in oxygen fugacity between the standard and the unknown will be too small (i.e., if the standard has an oxygen fugacity higher than that of the unknown, the value calculated for the unknown will be erroneously high).

The f_{O_2} at which electronic conduction becomes a serious

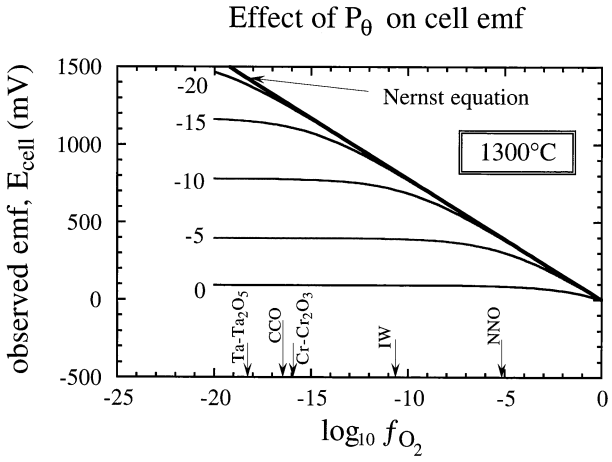

Fig. 2. Effect of P_θ on E_{cell} at 1300°C as a function of $log_{10} f_{O_2}$. Labels adjacent to curves are values of log P_θ. Also shown are calculated oxygen fugacities at 1300°C for the buffers Cr-Cr_2O_3 (Holzheid and O'Neill, 1995), CCO, Ta-Ta_2O_5 (Robie et al., 1979), IW, and Ni-NiO (O'Neill and Pownceby, 1993). Note that the oxygen fugacities considered here and in the text are referenced to pure O_2 gas at a pressure of 1 bar.

problem varies with temperature and the electrolyte material. The effect can be described by

$$E_{cell} = \frac{-RT}{F} ln \left\{ \frac{(P_\theta^{1/4} = f_{O_2@B}^{1/4})}{(P_\theta^{1/4} + f_{O_2@A}^{1/4})} \right\}, \quad (2)$$

where P_θ is the oxygen fugacity at which half of the conductivity is due to electronic conduction. This expression was first obtained by Schmalzried (1962, 1963) based on the treatment of Wagner (1933). Deviations from the Nernst equation can thus be described at constant temperature in terms of a single constant, P_θ, independent of oxygen fugacity. When written in this form, which is comparable to that of Eqn. 1 for the case of purely ionic conduction, the nature of the correction for electronic conduction becomes apparent. The larger P_θ is, the higher the oxygen fugacity for which significant deviations from the Nernst equation will occur, as shown in Fig. 2 . It is also worth noting from this figure that at any given P_θ, the sensitivity of E_{cell} to deviations from the Nernst equation is greatest when f_{O_2} is within 3 log units of P_θ. It is in this region that the most accurate determinations of P_θ are possible. Under more reducing conditions, E_{cell} becomes a weak function of f_{O_2} and, under more oxidizing conditions, deviations from the Nernst equation are too small. Figure 2 also has implications for the inverse problem, the solution of which is a primary goal of this study: for a set of values of P_θ, $f_{O_2@A}$, and E_{cell}, calculate $f_{O_2@B}$. Given some uncertainty in P_θ, flattening of the curves in Fig. 2 under reducing conditions implies that the uncertainty in such a calculation increases rapidly with decreasing f_{O_2} and is very large when f_{O_2} is more than ~3 log units below P_θ (i.e., the correction to the Nernst equation is large in a redox regime where E_{cell} is relatively insensitive to f_{O_2}). As the f_{O_2} is increased from these low levels, both the size of the correction and the relative error in determining it become smaller.

It is important to note that Eqn. 2 assumes electronic conduction to be the only cause of deviations from the ideal form of the Nernst equation. We show below that cell emfs for $SIRO_2$® oxygen sensors under reducing conditions outside the range of purely ionic conduction are in fact described reasonably well by Eqn. 2. Thus, other processes such as diffusion of O_2 molecules through the alumina along cracks or grain boundaries, slow transport of oxygen through the porous Pt electrode, reduction of the electrolyte, or some form of contact resistance, either do not contribute significantly to the cell emf or, coincidentally, do so in a manner consistent with Eqn. 2. If these or other factors are important contributors to the observed cell emfs, then inferred values of P_θ should be viewed as empirical constants.

Rearranging Eqn. 2 leads to

$$ln\, f_{O_2@B} = \frac{-4E_{cell}F}{RT} + ln\, f_{O_2@A} + 4\, ln \left\{ 1 + \left(1 - exp\left[\frac{E_{cell}F}{RT} \right] \right) \left(\frac{P_\theta}{f_{O_2@A}} \right)^{1/4} \right\}, \quad (3)$$

which presents f_{O_2} of the unknown gas as an explicit function of P_θ. The main purposes of this study are to determine values of P_θ for $SIRO_2$® sensors as a function of temperature and to establish a simple calibration procedure for solid electrolyte oxygen sensors. Given this information, Eqn. 3 can be used as the operative equation for the determination of oxygen fugacities in experimental gas mixtures under reducing conditions.

2. EXPERIMENTAL TECHNIQUES

Experiments were conducted in a vertical 1 atm gas-mixing furnace with $MoSi_2$ heating elements. We used YSZ oxygen sensors ($SIRO_2$®), obtained from Ceramic Oxide Fabricators, Ltd., Eaglehawk, Australia and Pt electrodes. These sensors (Figs. 1, 3) consist of an electrolyte plug, a two-phase mixture of alumina plus YSZ (9.5 mol% Y_2O_3), inserted into one end of an alumina tube and welded to form a gas tight seal (Badwal et al., 1987). Temperatures were monitored using a Pt-Pt10Rh thermocouple located inside the oxygen sensor, the Pt leg of which also acted as the internal lead for the oxygen cell. Graphite (used in some cases to fix the gas composition; see below) was commercial grade (Ultra®carbon, 99.8%). Metal for calibration consisted of 1.0 mm OD Ta wire (Alfa®, 99.97%), 0.23 mm OD Fe wire (Baker analyzed®, 99.9%) and Cr flakes cut into strips (Alfa®, 99.99%). The relatively thick Ta wire was necessitated by its high evaporation rate in our experiments.

2.1. Resistance Technique

The first type of experiment (Fig. 4a) was used to locate the Fe-wüstite (IW), Cr-Cr_2O_3, and Ta-Ta_2O_5 buffer curves. This procedure has been used in our laboratory at Caltech for confirming Nernstian behavior of oxygen sensors for some time (e.g., Beckett et al., 1988). It is based on the much higher resistance of the oxide of an element relative to that of the pure metal. Two thick Pt wires, typically 0.76 mm in diameter are threaded through the holes in an alumina tube (we use 4-bore, 6.4 mm OD alumina tubes from McDanel Vesuvius, Malvern, PA for this purpose). At the end of the alumina tube to be exposed at high temperatures, the Pt wires are bent into hooks. A Pt wire 0.33 mm in diameter and approximately 2.5 cm long is then wrapped around each of the hooks such that roughly 1 cm extends beyond the bottom. A metal wire of the material to be used for calibration is then spot welded (Fe, Ta, ±Cr) to the 0.33 mm OD Pt wire or, for some of the Cr wafers, the Pt wire was welded to the metal strip using an H_2-O_2 torch. This results in the arrangement shown in Fig. 4a. The opposite ends of the thick Pt wires extend above the furnace where they can be attached to an ohmmeter and the resistance of the circuit measured. Prior to beginning a calibration experiment, the

sample assembly contain ing
the oxygen sensor is set up such that upon
insertion into the furnace, the tip of the thermocouple inside the sensor tube is in the hot spot but the welded wire is suspended ~5 cm below the top of the furnace in a cooler zone. The furnace is then flushed with N_2, and the sample assembly inserted into the furnace under flowing N_2. Once the system stabilizes to a constant temperature, the N_2 is turned off. For Fe and Ta experiments, an H_2-CO_2 gas more reducing than the oxide-metal buffer is introduced. Once a stable cell emf is achieved in a matter of minutes, the wire is inserted into the hot spot and the system again allowed to stabilize. The CO_2/H_2 ratio of the gas is then increased until an increase in the resistance across the Fe or Ta wire is observed. This indicates that an oxide is forming on the wire and hence that the flowing gas lies within the stability field of the oxide (i.e., at conditions more oxidizing than the buffer curve). The CO_2/H_2 ratio of the gas was then decreased until the resistance again decreased, indicating that the f_{O_2} of the vapor had crossed that of the buffer curve and now lay in the stability field of the metal. By iterating this reversal from metal → oxide → metal in successively smaller increments of gas composition, it was possible to bracket the emf corresponding to the position of the metal-oxide buffer to within 1 mV. Ta wires usually failed due to evaporation of the metal after measurements at two or three temperatures. Iron wires could be used in many measurements without loss, although for measurements below 1200°C, it was necessary to pass the mixed gas through a Pt catalyst to ensure equilibration within the vapor (see Beckett and Mendybaev, 1997). For Cr, the initial nucleation of oxides on the water is very slow, and the water was, therefore, inserted into the hot spot at 1400 or 1500°C under flowing air and held there until the oxidation began as evidenced by an increased resistance. This initial incubation period lasted from a few hours to a day but, once nucleated, the amount of Cr_2O_3 and hence the resistance could be manipulated through changing gas composition. The experiment then proceeded as above for Ta and Fe. Individual Cr strips cut from the Cr flakes generally yielded measurements at three or four temperatures before failing.

Contamination of the metal wires by Pt potentially introduces an error because the oxygen fugacity for equilibrium between the resulting alloy and an oxide is higher than that of the pure metal-oxide. For Fe and Ta, this effect is negligible in our experiments because exposure times in the temperature range 1200–1400°C are only a few hours, and the resistances are, therefore, dominated by oxides in contact with pure metal. For Cr, however, exposure times at high temperatures were often much longer due to the initial oxidation step. This resulted in the formation of an intermetallic phase, Cr_3Pt, at the interface between Cr and Pt and ~20 wt% Pt in the Cr wafer at the contact. Were the entire wafer characterized by such a high concentration of Pt, the alloy-oxide equilibrium would be two log units more oxidizing than the Cr-Cr_2O_3 buffer (using activity-composition data for Cr-Pt alloys of Kay and Mohanty (1970) and free energy data of Holzheid and O'Neill, 1995), and, therefore, calculated values of P_θ based on the Cr-O system would be grossly in error. To test this possibility, we measured relative flow rates of H_2 and CO_2 in mixed gases at metal-oxide equilibrium using the floating soap film technique described by Nafziger et al. (1971). Observed values of 0.38–0.41 vol% CO_2 for Cr_2O_3 in equilibrium with our Cr wafers at 1400°C correspond to $log_{10} f_{O_2} = -14.44 \pm 0.04$ based on the gas mixing tables of Deines et al. (1974), in excellent agreement with $log_{10} f_{O_2} = -14.50$ obtained from the free energy of formation of Cr_2O_3 given by Holzheid and O'Neill (1995). The agreement implies that Pt contamination does not contribute significantly to our results, even for Cr, and our resistance technique, therefore, captures the position of the pure metal-oxide equilibrium for each of the elements studied. We note that mixed gases of known composition can

Fig. 3. Backscattered electron photomicrograph of $SIRO_2$® oxygen sensor. The region in the lower portion of the figure is part of the alumina tube with alumina (dark) and interstitial YSZ (bright). The central portion shows eutectic intergrowths characteristic of the welded region, and the upper portion displays the alumina-YSZ mixture of the electrolyte. There is also a large arcuate crack near the interface between the welded zone and the alumina/YSZ electrolyte plug, which may have been a factor in the failure of this sensor.

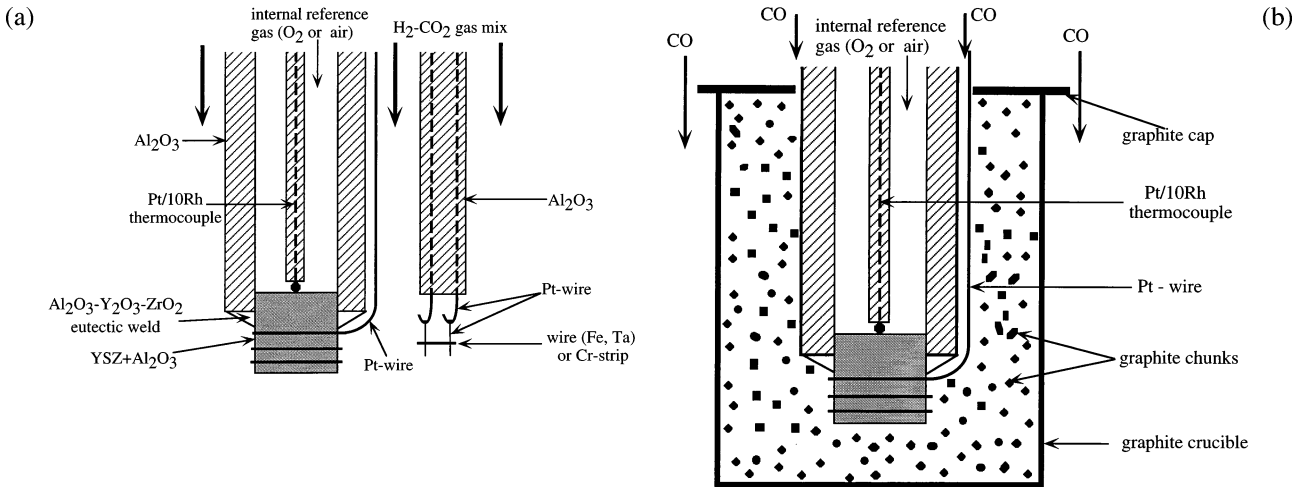

Fig. 4. Schematics of calibration set-up. (a) Bare wire (Fe or Ta) or strip cut from a flake (Cr) used for IW, Cr-Cr_2O_3, and Ta-Ta_2O_5 buffer calibrations. (b) Graphite capsule.

be used to indirectly calibrate deviations from Nernstian behavior as shown above for Cr-Cr_2O_3 (see also Burkhard and Ulmer (1995) and references therein). We chose not to pursue this approach, except as a check for internal consistency, because (1) for flow rates corresponding to less than ~0.1 vol% CO_2, errors on the flow rates were a substantial fraction of the flow rate, and (2) at very high mixing ratios (i.e., under very reducing conditions), contaminants in the hydrogen significantly influenced the oxygen fugacity (i.e., vapor compositions did not lie precisely on the H_2-CO_2 binary). Both of these problems can be overcome though at considerable expense.

2.2. Graphite Capsule Technique

An alternative procedure was used to determine the emf corresponding to the graphite-gas coexistence in the C-O system (referred to as the ''CCO'' buffer; Fig. 4b). First, a hole 1.1 cm in diameter was drilled into a 16 mm OD, 4 cm long graphite rod to form a crucible. A cap of the same material was then cut with a central hole to accommodate the oxygen sensor tube and an additional, off-center hole to allow passage of the external electrode. With the oxygen sensor fixed in place, mounted in the top plate assembly, the cap and crucible were brought up from underneath the sensor and slid up over its end. The cap was then slid further up to expose the cavity between the crucible and sensor and the cavity filled with 2–3 mm diameter graphite chips. The cap was then slid back into place to cover the crucible resulting in the arrangement depicted schematically in Fig. 4b. The graphite crucible was secured by Pt wire to Pt hooks suspended from an adjacent alumina rod (cf. Fig. 4a). The assembly was placed into the furnace under flowing N_2 at 1000°C. The N_2 was then turned off and CO introduced into the furnace. A stable emf then corresponded to the value for the CCO buffer at that temperature. Although some degradation of the graphite capsule occurred with time, it was possible to measure emfs at several temperatures using one capsule.

3. RESULTS

3.1. Calibration of the YSZ Sensor

Figure 5 shows results of calibration measurements for one sensor obtained at IW, Cr-Cr_2O_3, CCO, and Ta-Ta_2O_5 together

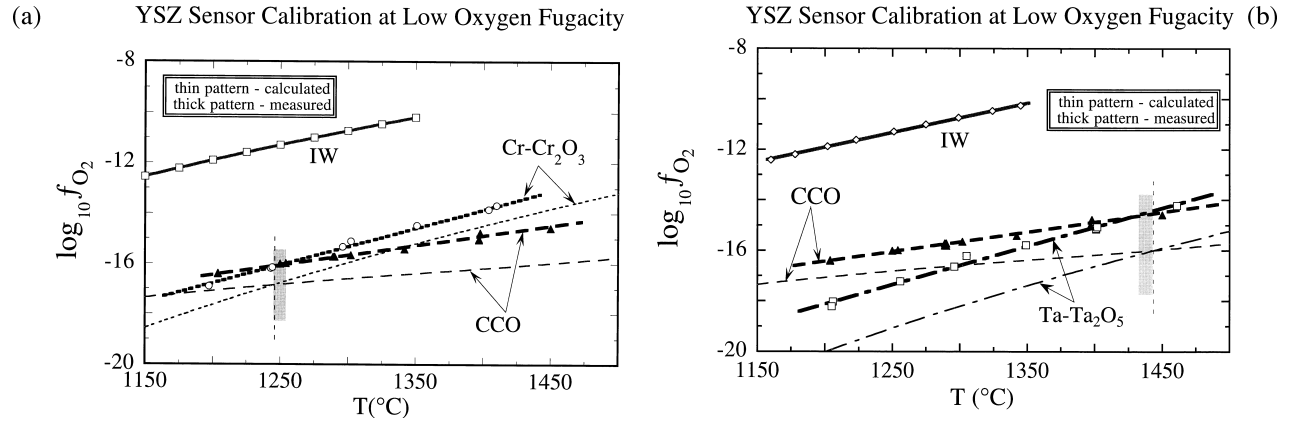

Fig. 5. Calibration data for SIRO$_2$® sensor. Apparent values of $log_{10}f_{O_2}$ calculated from our emf measurements using the Nernst equation with air as the reference gas are plotted against temperature. Also shown are the corresponding positions of buffer curves according to the literature (CCO and Ta-Ta_2O_5: Robie et al., 1979; IW: O'Neill and Pownceby, 1993; Cr-Cr_2O_3: Holzheid and O'Neill, 1995). The vertical dashed lines refer to the temperature of intersection for the calculated buffer curves with shading corresponding to the 1σ uncertainty band on the intersection of the experimentally determined equilibria. Nominal errors on the measurements are smaller than the symbol sizes. (a) IW, CCO and Cr-Cr_2O_3. (b) IW, CCO and Ta-Ta_2O_5.

with buffer curves calculated based on thermodynamic data. Individual symbols correspond to apparent oxygen fugacities calculated using the ideal form of the Nernst equation (Eqn. 1). Vertical dashed lines indicate temperatures at which the calculated buffer curves intersect. There are three important features. (1) For a given buffer assemblage, the apparent $log_{10}f_{O_2}$ values based on the Nernst equation vary approximately linearly with temperature but differ systematically from calculated values for the same buffer assemblage. This is a direct measure of the error introduced by assuming that the Nernst equation is correct. The results are reproducible despite cycling of the sensor up and down temperature, varying the order in which different buffer assemblages were used, and, for Cr-Cr_2O_3, varying the length of the initial oxidation step. This implies that time dependent processes such as diffusion of Pt into the metal or of the metal into the Pt support wires did not affect the results. (2) The deviation at constant temperature between calculated and actual oxygen fugacity as determined by the buffer assemblage is nearly zero for IW ($log_{10}f_{O_2}$ obtained using Eqn. 2 and values calculated from Huebner (1971) agree within ± 0.02) but increases systematically with decreasing f_{O_2} (i.e., for this experimental setup where the reference gas is well inside the Nernstian regime). Thus, at a given temperature, the error in assuming that the ideal form of the Nernst equation is correct becomes larger as the oxygen fugacity is decreased. (3) The temperatures at which the measured Cr-Cr_2O_3 and Ta-Ta_2O_5 buffer curves intersect the CCO curve (shown as shaded boxes in Fig. 5) are within 2σ, as determined from propagation of errors on the linear regressions, of the intersection based on the thermodynamic calculations (1250 ± 6 (1σ) vs. 1245°C (Robie et al., 1979; Holzheid and O'Neill, 1995) and 1432 ± 9 (1σ) vs. 1444°C (Robie et al., 1979); see vertical dashed lines) even if uncertainties in the thermodynamic calculations are not considered. This is an important statement of internal consistency.

Rearranging Eqn. 3 leads to

$$P_\theta = \left\{ \frac{f_{O_2@B}^{1/4}\, exp\left(\frac{E_{cell}F}{RT}\right) - f_{O_2@A}^{1/4}}{1 - exp\left(\frac{E_{cell}F}{RT}\right)} \right\}^4. \qquad (4)$$

Thus, each measurement of a cell emf at a known temperature and oxygen fugacity (i.e., along a buffer curve for our experiments) generates a value of P_θ. Calculated values based on our measurements of the Cr-Cr_2O_3, CCO, and Ta-Ta_2O_5 buffers are shown in Fig. 6. Values based on the IW buffer are inappropriate for determining P_θ because deviations between the measured and calculated (based on thermochemical data) positions of the buffer curve are too small (i.e., uncertainties in the measurements and in the calculated buffer curve exceed deviations from the Nernst equation). That deviations from the Nernst equation are small for the IW buffer is well known (Sato, 1971) and is the basis for using this buffer as a calibration point for some oxygen sensors (e.g., Williams and Mullins, 1981; Beckett et al., 1988). In contrast, deviations from the standard form of the Nernst equation greatly exceed uncertainties in measurement or thermodynamic data for the CCO, Cr-Cr_2O_3 and Ta-Ta_2O_5 buffer assemblages at 1 bar. A linear

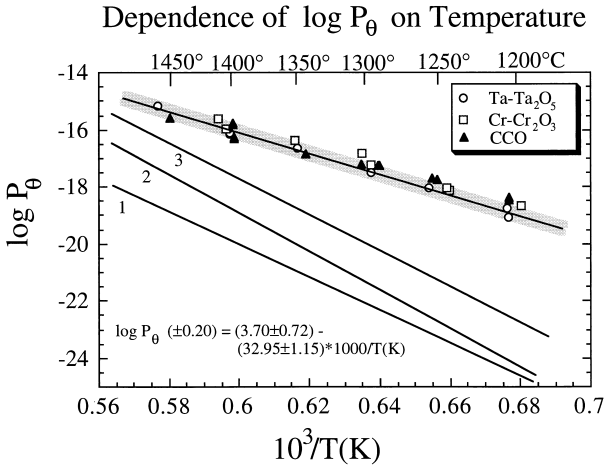

Fig. 6. log_{10} P_θ vs. 10^3/T(K). Each symbol represents one determination of the emf for an $SIRO_2$® oxygen sensor (9.5 mol% Y_2O_3-doped ZrO_2) corresponding to a particular buffer assemblage using air as the reference gas. Determinations of P_θ from the literature are also shown with data sources indicated. (1) Polarization measurement on 7 mol% Y_2O_3-doped ZrO_2 (Swinkels, 1970). (2) Coulometric titration on 6 and 8 mol% Y_2O_3-doped ZrO_2 (Sasabe et al., 1991). (3) Bipolar impedance measurements on 6 and 8 mol% Y_2O_3-doped ZrO_2 (Sasabe et al., 1991).

regression of our data for these three buffers is shown in Fig. 6 and is given by the following equation:

$$log_{10}P_\theta(\pm 0.20) = 3.70(\pm 0.72) - \frac{(32.95 \pm 1.15) \times 10^3}{T(K)}. \qquad (5)$$

where quoted uncertainties are 1σ. Also shown are measurements of $log_{10}P_\theta$ from the literature obtained for single-phase YSZ (Swinkels, 1970; Sasabe et al., 1991). Our calculated values of $log_{10}P_\theta$ for $SIRO_2$® sensors are significantly higher than the reported values for single-phase YSZ. In part, this reflects the presence of large amounts of alumina (50 wt%) in the electrolyte of $SIRO_2$® sensors. According to a simple treatment of conductivity in multiphase aggregates (Kingery et al., 1976), which is consistent with results for 0–30 wt% alumina in YSZ (Ishizaki et al., 1989), this can be expected to reduce the ionic conductivity by a factor of ~3.5, leading to an increase of 2 in $log_{10}P_\theta$ relative to pure YSZ. Additional contributions arise from differences in grain size (scaling with surface area of grain boundaries), and, in fact, resistivity measurements of Badwal (1987) on single phase YSZ and $SIRO_2$® electrolyte suggest that the difference in $log_{10}P_\theta$ should be ~4, consistent with observation (Fig. 6). That the slopes of lines for single-phase YSZ significantly differ from our determination may reflect differences in the relative contributions of grain boundaries and interiors to the total conductivity. It is also worth noting in this context that scatter of data about some of the lines in Fig. 5 significantly exceeds expectations based on the nominal uncertainties (smaller than symbol sizes) and that the scatter tends to increase with decreasing f_{O_2} (compare IW with Ta-Ta_2O_5 in Fig 5b). One possibility is that electrode-electrolyte reactions occur in our experiments on the low f_{O_2} side of the sensor, producing one or more PtZr intermetallic compounds (Lu et al., 1995) and introducing an additional voltage

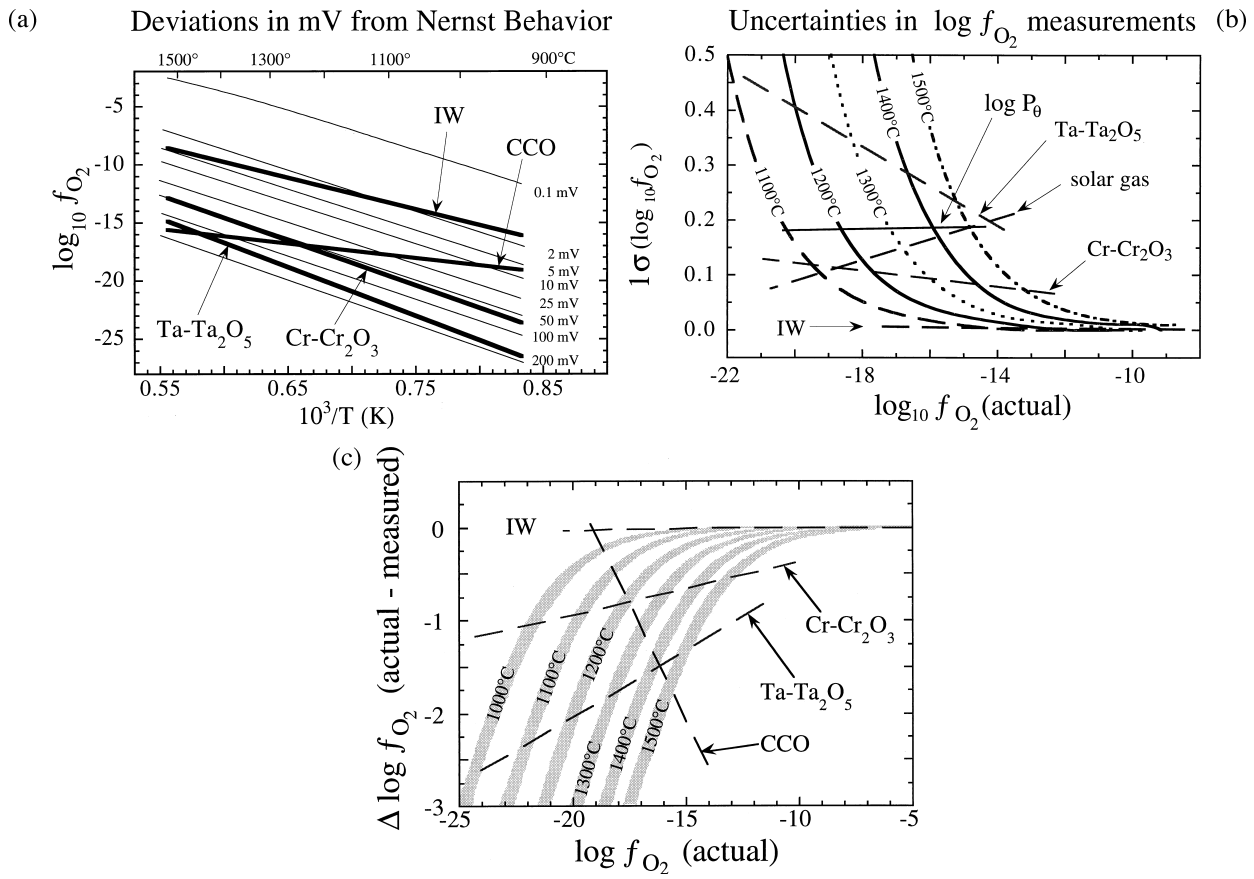

Fig. 7. Errors and uncertainties associated with use of the ideal form of the Nernst equation (Eqn. 1) and corrections for electronic conduction calculated using Eqns. (3–5). An air reference is assumed for the sensor. Literature sources for buffer curves are as in Fig. 5. (a) $log_{10}f_{O_2}$ at which electronic conduction accounts for a specified number of mV. (b) Deviation (1σ) in $log_{10}f_{O_2}$ due to uncertainties in P_θ as a function of $log_{10}f_{O_2}$ at specified temperatures. The position of P_θ was calculated using data from this study. The curve labelled ''solar gas'' refers to a gas of solar composition whose T-f_{O_2} relationship was calculated from solar abundances (Anders and Grevesse, 1989) and thermodynamic data for gaseous species taken from Chase et al. (1985). It was assumed that this vapor is an ideal gas mixture. (c) Difference between apparent (ideal Nernst) and actual $log_{10}f_{O_2}$ as a function of the actual $log_{10}f_{O_2}$.

to the cell. Alternatively, modest effects may be caused by the evaporation of graphite, Fe, Ta, and/or Cr during calibration, leading to contamination of the Pt lead and the introduction of a thermal emf contribution (e.g., Iwase et al., 1984b). None of these effects are taken into account by the analysis in this work, and, if one or more of them is important, the interpretation of our values for P_θ as indicating the f_{O_2} at which electronic and ionic conductivities are equal would be incorrect in detail. Equations 3 and 5 could, nonetheless, still be used to determine $log_{10}f_{O_2}$ because they reflect deviations from the ideal form of the Nernst equation as they exist for the operating oxygen sensor.

We tested five SIRO$_2$® oxygen sensors taken from several different batches of SIRO$_2$® sensors purchased over about a decade against the calibrated sensor described above (i.e., the two sensors were exposed simultaneously to the same vapor at the same temperature). All of the results are consistent within ±3 mV, well within the uncertainties quoted for Eqn. 5 (i.e., Eqn. 5 is a good representation for all SIRO$_2$® YSZ oxygen sensors using our experimental configuration). However, since several factors may influence the electronic conductivity of a particular sensor (and thus the actual deviation of a particular sensor from Nernstian behavior), it would probably be desirable, given one calibrated sensor as a secondary standard, to calibrate other oxygen sensors against it by simultaneously exposing the standard and new oxygen sensor to the same reducing gas. We also emphasize that our measurements are directly applicable only to SIRO$_2$® oxygen sensors. It is highly unlikely that Eqn. 5 would provide even a crude approximation for other types of YSZ oxygen sensors (cf. Fig. 6). The calibration procedures described above are, however, equally applicable to these materials.

3.2. Implications for Measurement of Oxygen Fugacities Using SIRO$_2$® Oxygen Sensors.

The oxygen fugacities at which electronic conduction accounts for 0.1–200 mV of the cell emf were calculated using Eqns. 3 and 5 and are shown in Fig. 7a. The correction is nominally observable even at IW but given that available determinations of the buffer curve (Huebner, 1971; Robie et al., 1979; Chase et al., 1985; O'Neill and Pownceby, 1993) vary

over ~10 mV, deviations implied by the figure, though likely real, are small enough so that no weight should be given to them in determining P_θ. On the other hand, deviations for CCO, Cr-Cr_2O_3, and Ta-Ta_2O_5 greatly exceed combined thermodynamic and experimental uncertainties in the temperature range 1200–1500°C. For Ta-Ta_2O_5, the deviations from Nernstian behavior correspond to more than 10% of E_{cell}.

Figure 7b gives the uncertainty in calculating $log_{10}f_{O_2}$ using Eqns. 3 and 5. Also shown are positions of the experimentally determined P_θ for this study, three metal-oxide buffers, and the T-f_{O_2} locus for a gas of solar composition. The uncertainty is negligible for IW because the correction is small, and the uncertainty at P_θ is still less than ± 0.2 log units. Thus, the f_{O_2} for a gas of solar composition below 1500°C can be determined to better than ± 0.2 log units (1σ). Under conditions more reducing than P_θ, the uncertainty increases rapidly, reaching ± 0.4 log units for Ta-Ta_2O_5 at 1200°C.

The range over which electronic conduction can be ignored and the ideal form of the Nernst equation safely used depends on the accuracy required of a given application. For typical gas mixing experiments under conditions more oxidizing than IW, the effect is negligible (<0.1 log units) in the temperature range of 1000–1500°C. At lower oxygen fugacities, however, the effect becomes progressively more serious (Fig. 7c). For the Ta-Ta_2O_5 buffer, the discrepancy is more than one log unit at 1500°C and nearly 3 log units at 1000°C. Calculation of $log_{10}f_{O_2}$ using Eqn. 3 and our determinations of P_θ (Eqn. 5) substantially reduces the error from this source (Fig. 7b).

Acknowledgments—This work was supported by NASA grants NAGW-3212, NAG5-6181, and NAG5-4318. Discussions with E. Kolaczyk and S. Song concerning the uncertainty in determining the intersection of two lines were very helpful and the reviews of J. S. Huebner and an anonymous reviewer lead to significant improvements. A. M. Davis and S. B. Simon are thanked for their help with the SEM and microprobe.

REFERENCES

Alcock C. B. (1993) Thermodynamic and transport properties of electroceramic oxide systems. *J. Alloys Comp.* **197,** 217–227.

Anders E. and Grevesse N. (1989) Abundances of the elements: Meteoritic and solar. *Geochim. Cosmochim. Acta* **53,** 197–214.

Arculus R. J. and Delano J. W. (1981) Intrinsic oxygen fugacity measurements: Techniques and results for spinels from upper mantle peridotites and megacryst assemblages. *Geochim. Cosmochim. Acta* **45,** 899–913.

Badwal S. P. S., Bannister M. J., and Garret W. G. (1987) Oxygen measurement with $SIRO_2$ sensors. *J. Phys. E: Sci. Instr.* **20,** 531–540.

Beckett J. R., Live D., Tsay F.-D., Grossman L., and Stolper E. (1988) Ti^{3+} in meteoritic and synthetic hibonite. *Geochim. Cosmochim. Acta* **52,** 1479–1495.

Beckett J. R. and Mendybaev R. A. (1997) The measurement of oxygen fugacities in flowing gas mixtures at temperatures below 1200°C. *Geochim. Cosmochim. Acta* **61,** 4331–4336.

Brett R. and Sato M. (1984) Intrinsic oxygen fugacity measurements on seven chondrites, a pallasite, and a tektite and the redox state of meteorite parent bodies. *Geochim. Cosmochim. Acta* **48,** 111–120.

Burkhard D. J. M. and Ulmer G. C. (1995) Kinetics and equilibria of redox systems at temperatures as low as 300°C. *Geochim. Cosmochim. Acta* **59,** 1699–1714.

Chase M. W., Jr., Davies C. A., Downey J. R., Jr., Frurip D. J., McDonald R. A., and Syverud A. N. (1985) The JANAF thermochemical tables, 3rd edition. *J. Phys. Chem. Ref. Data* **14** (Suppl. 1).

Deines P., Nafziger R. H., Ulmer G. C., and Woermann E. (1974) Temperature - oxygen fugacity tables for selected gas mixtures in the system C-H-O at one atmosphere total pressure. *Bull. Earth Mineral. Sci. Expt. Station* **88,** 1–129.

Etsell T. H. and Flengas S. N. (1970) The electrical properties of solid oxide electrolytes. *Chem. Rev.* **70,** 339–376.

Holzheid A. and O'Neill H., St.C. (1995) The Cr-Cr_2O_3 oxygen buffer and the free energy of formation of Cr_2O_3 from high-temperature electrochemical measurements. *Geochim. Cosmochim. Acta* **59,** 475–479.

Huebner J. S. (1971) Buffering techniques for hydrostatic systems at elevated pressures. In *Research Techniques for High Pressure and High Temperature* (ed. G. C. Ulmer), pp. 123–177. Springer-Verlag.

Huebner J. S. (1987) Use of gas mixtures at low pressure to specify oxygen and other fugacities of furnace atmospheres. In *Hydrothermal Experimental Techniques* (ed. G. C. Ulmer and H. L. Barnes), pp. 20–60. Wiley.

Ishizaki F., Yoshida T., and Sakurada S. (1989) Effect of alumina additions on the electrical properties of yttria doped zirconia. In *Proceedings of the First International Symposium on Solid Oxide Fuel Cells* (ed. S. C. Singhal), pp. 3–14. The Electrochemical Society.

Iwahara H. and Hibino T. (1993) New gas sensors using high temperature proton conducting ceramics. In *Proceedings of the Symposium on Chemical Sensors II* (ed. M. Butler, A. Ricco, and N. Yamazoe), pp. 464–473. The Electrochemical Society.

Iwase M., Ichise E., and Jacob K. T. (1984a) Mixed ionic and electronic conduction in zirconia and its application in metallurgy. In *Advances in Ceramics, vol. 12, Science and Technology of Zirconia II* (ed. N. Claussen et al.), pp. 646–659. American Ceramic Society.

Iwase M., Ichise E., Takeuchi M., and Yamasaki T. (1984b) Measurements of the parameter, P_θ, for the determinations of mixed ionic and n-type electronic conduction in commercial zirconia electrolytes. *Trans. Japan Inst. Metals* **25,** 43–52.

Jacob K. T. and Iwase M. (1983) Effect of pressure on the emf of solid-state cells. *High Temp. Sci.* **16,** 123–129.

Kay D. A. R. and Mohanty A. K. (1970) The thermodynamic properties of some Pt-Cr alloys in the temperature range 1450–1550°C. *Metall. Trans.* **1,** 303–304.

Kingery W. D., Bowen H. K., and Uhlmann D. R. (1976) *Introduction to Ceramics*. Wiley.

Kiukkola K. and Wagner C. (1957) Measurements on galvanic cells involving solid electrolytes. *J. Electrochem. Soc.* **104,** 379–387.

Kofstad P. (1983) *Nonstoichiometry, diffusion, and electrical conductivity in binary metal oxides*. Robert E. Krieger Publ. Co.

Kozul J. M., Ulmer G. C., and Hewins R. H. (1988) Intrinsic oxygen fugacity measurements of some Allende Type B inclusions. *Geochim. Cosmochim. Acta* **52,** 2707–2716.

Lu F.-H., Newhouse M. L., Dieckmann R., and Xue J. (1995) Platinum: A noninert material reacting with oxides. *Sol. State Ionics* **75,** 187–192.

Nafziger R. H., Ulmer G. C., and Woermann E. (1971) Gaseous buffering for the control of oxygen fugacity at one atmosphere. In *Research Techniques for High Pressure and High Temperature* (ed. G. C. Ulmer), pp. 9–41. Springer-Verlag.

Naito H. and Arashi H. (1992) Electrical properties of ZrO_2-TiO_2-Y_2O_3 system. *Sol. State Ionics* **53–56,** 436–441.

O'Neill H., St.C. and Pownceby M. I. (1993) Thermodynamic data from redox reactions at high temperatures. I. An experimental and theoretical assessment of the electrochemical method using stabilized zirconia electrolytes, with revised values for the Fe-"FeO", Co-CoO, Ni-NiO and Cu-Cu_2O oxygen buffers, and new data for the W-WO_2 buffer. *Contrib. Mineral. Petrol.* **114,** 296–314.

O'Neill H., St.C., Pownceby M. I., and Wall V. J. (1989) Activity-composition relations in $FeTiO_3$ - $MnTiO_3$ ilmenite solid solutions from EMF measurements at 1050-1300K. *Contrib. Mineral. Petrol.* **103,** 216–222.

Pandit S. S., Weyl A., and Janke D. (1994) High-temperature ionic and electronic conduction in zirconate and hafnate compounds. *Sol. State Ionics* **69,** 93–99.

Park J.-H. and Blumenthal R. N. (1989) Thermodynamic properties of nonstoichiometric yttria-stabilized zirconia at low oxygen pressures. *J. Amer. Ceramic Soc.* **72,** 1485–1487.

Patterson J. W. (1971) Conduction domains for solid electrolytes. *J. Electrochem. Soc.* **118,** 1033–1039.

Pratt J. N. (1990) Applications of solid electrolytes in thermodynamic studies of materials: A review. *Metall. Trans.* **21A,** 1223–1250.

Ramanarayanan T. A., Ling S., and Anderson M. P. (1991) Electrochemical analysis of mixed conductions in ceramic oxide membranes. In *Proceedings of the 1st International Symposium on Ionic and Mixed Conduction Ceramics* (ed. T. A. Ramanarayanan and H. L. Tuller), pp. 110–121. The Electrochemical Society.

Robie R. A., Hemingway B. S., and Fisher J. R. (1979) Thermodynamic properties of minerals and related substances at 298.15K and 1 bar (10^5 Pascals) pressure and at higher temperatures. *U.S. Geol. Surv. Bull.* **1452,** 1–456.

Rommerskirchen I., Chávez F., and Janke D. (1994) Ionic conduction behavior of mullite ($3Al_2O_3 \cdot 2SiO_2$) at 1400–1600°C. *Sol. State Ionics* **74,** 179–187.

Sasabe M., Miyashita M., Hua J. Z., and Senoo H. (1991) Determination of a partial electronic conduction parameter of solid electrolytes for an oxygen sensor by using A.C. two terminals method. *Tetsu to Hagane* **77,** 790–797 (in Japanese).

Sato M. (1971) Electrochemical measurements and control of oxygen fugacity and other gaseous fugacities with solid electrolyte sensors. In *Research Techniques for High Pressure and High Temperature* (ed. G. C. Ulmer), pp. 43–99. Springer-Verlag.

Sato M. (1972) Intrinsic oxygen fugacities of iron-bearing oxide and silicate minerals under low total pressure. *Geol. Soc. Amer. Mem.* **135,** 289–307.

Schmalzried H. (1962) Über Zirkondioxyd als Electrolyt für electrochemische Untersuchungen bei höheren Temperaturen. *Z. Elektrochem.* **66,** 572–576.

Schmalzried H. (1963) Ionen- und Elektronenleitung in binären Oxiden und ihre Untersuchung mittels EMK-Messungen. *Z. Phys. Chem. n. Folge* **38,** 87–102.

Smyth D. M. (1976) Thermodynamic characterization of ternary compounds. I. The case of negligible defect association. *J. Solid State Chem.* **16,** 73–81.

Smyth D. M. (1977) Thermodynamic characterization of ternary compounds. II. The case of extensive defect association. *J. Solid State Chem.* **20,** 359–364.

Subbarao E. C. and Maiti H. S. (1984) Solid electrolytes with oxygen ion conduction. *Sol. State Ionics* **11,** 317–338.

Sutija D. P., Norby T., and Björnbom P. (1995) Transport number determination by the concentration-cell/open-circuit voltage method for oxides with mixed electronic, ionic, and protonic conduction. *Sol. State Ionics* **77,** 167–174.

Swider K. E., Laughin S., and Worrell W. L. (1991) Investigation of the electronic conduction mechanism in yttria-stabilized zirconia-titania. In *Proceedings of the 1st International Symposium on Ionic and Mixed Conduction Ceramics* (ed. T. A. Ramanarayanan and H. L. Tuller), pp. 73–83. The Electrochemical Society.

Swinkels D. A. J. (1970) Rapid determination of electronic conductivity limits of solid electrolytes. *J. Electrochem. Soc.* **117,** 1267–1268.

Ulmer G. C. (1984) ZrO_2 oxygen and hydrogen sensors: A geologic perspective. In *Science and Technology of Zirconia II* (ed. N. Claussen, M. Rühle, and A. H. Heuer); *Adv. Ceram.* **12,** 660–671. American Ceramic Society.

van Wijngaarden M. J. U. T., Geldenhuis J. M. A., and Dippenaar R. J. (1988) An experimental technique employing a high-temperature gas-tight alumina seal for the assessment of the electrical properties of solid electrolytes. *J. Appl. Electrochem.* **18,** 724–730.

Wagner C. (1933) Beitrag zur Theorie des Anlaufvorgangs. *Z. Phys. Chem.* **B21,** 25–41.

Weissbart J. and Ruka R. (1961) Oxygen gauge. *Rev. Sci. Instr.* **32,** 593–595.

Williams R. J. and Mullins O. (1981) JSC systems using solid ceramic oxygen electrolyte cells to measure oxygen fugacities in gas-mixing systems. NASA Techn. Mem. 58234.

Woermann E., Stier B., and Rosenhauer M. (1982) The oxygen membrane cell - a device for controlling the oxygen fugacity in water-free high pressure systems. In *High-Pressure Researches in Geoscience* (ed. W. Schreyer), pp. 519–528. E. Schweizerbart'sche Verlagsbuchandlung.

Worrell W. L. (1977) Oxide solid electrolytes. In *Solid Electrolytes* (ed. S. Gellar); *Topics Appl. Phys.* **21,** 143–168.

Wu L., Wu C.-C. G., and Chang Y.-B. (1992) Electrical behavior of ZrO_2-MgO-Y_2O_3 solid electrolyte. *J. Electron. Mater.* **21,** 217–222.

Yasuda A. and Fujii T. (1993) Application of a solid-electrolyte oxygen fugacity sensor to high pressure experiments. *Phys. Earth Plan. Intl.* **80,** 49–64.